PROCEEDINGS OF THE ROYAL SOCIETY A

rspa.royalsocietypublishing.org

Research

Article submitted to journal

Subject Areas:
Ocean Engineering

Keywords:
wave farm modelling, wave-structure interaction, wave energy

Author for correspondence:
Dripta Sarkar
e-mail:
dripta.sarkar.1@ucdconnect.ie

Wave farm modelling of Oscillating Wave Surge Converters

Dripta Sarkar[1], Emiliano Renzi[1] and Frederic Dias[1]

[1]UCD School of Mathematical Sciences, University College Dublin, Ireland

A mathematical model is described to analyse the hydrodynamic behaviour of a wave energy farm consisting of oscillating wave surge converters in oblique waves. The method is a highly efficient semi-analytical approach based on the linear potential flow theory. Wave farms with a large number of such devices are studied for various configurations. For an inline configuration with normally incident waves, the occurrence of a near resonant behaviour, already known for small arrays, is confirmed. A strong wave focussing effect is observed in special configurations comprising of a large number of devices. The effects of the arrangement and of the distance of separation between the flaps are also studied extensively. In general, the flaps lying on the front of the wave farm are found to exhibit an enhanced performance behaviour in average, due to the mutual interactions arising within the array. The hydrodynamics of two flaps that oscillate back to back is also discussed.

1. Introduction

Wave farms comprising of a large number of wave energy converters (WECs) are planned at sites which have already been identified for the purpose of energy extraction (e.g. Lewis Wave Project, see [1]). The arrangement of the devices in such a farm can follow several possible configurations. The present study analyses the interaction of waves with an array of oscillating wave surge converters (OWSCs) and the performance of such systems. The OWSC considered here is a bottom hinged flap-type WEC which extracts energy by virtue of its pitching motion and resembles the Oyster® developed by Aquamarine Power Ltd.

Royal Society Publishing
Informing the science of the future

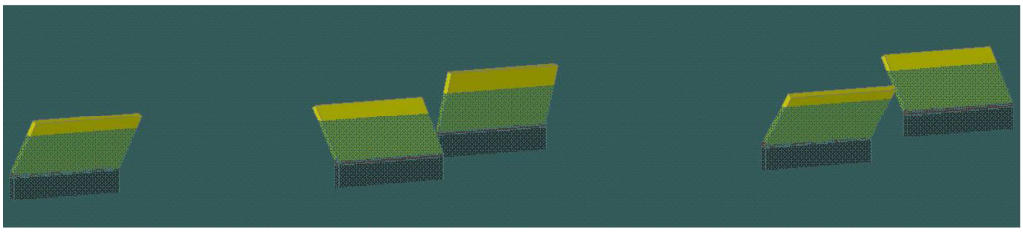

Figure 1. A computer generated 3D graphical view of a portion of a wave farm comprising of five OWSCs.

Wave power absorption in an array has already been studied in the literature, starting with the seminal work of [2]. However, the majority of the investigations deal with the hydrodynamics of point absorbers, which is based on the assumption that the body dimensions are much smaller than the wavelength of the incident wave field. Recent studies have shown that for OWSCs like Oyster, the point absorber limit is no longer applicable and hence better and more accurate modelling of the device needs to be undertaken [3]. Some recent investigations also dealt with a detailed analysis of multiple WECs, but most of them did not go beyond three or four of such devices ([4], [5], [6], [7]). Indeed, in the literature there have been very few attempts to understand the dynamics of large arrays. The analytical modelling of large and complex systems becomes difficult, while numerical approaches on the other hand are computationally expensive and performing such an analysis experimentally is quite challenging. Recently, [8] used a fast multipole accelerated linearised boundary element method to study large arrays of sparsely distributed generic WECs in deep water. However, despite the recent effort of [9], who devised a new method to investigate the hydrodynamics of a small inline array of OWSCs, to date there is still a need for an unifying theory of large arrays of OWSCs in any configuration and in oblique waves. The analysis in this paper extends the semi-analytical work of [9] to investigate a large farm of OWSCs in any configuration under oblique incident waves.

A mathematical model is developed here within the framework of linear potential theory. The theory allows the analysis of arbitrary configurations of an array of OWSCs, the only constraint being that all the converters have parallel pitching axes (see figure 1). The problem is formulated as a boundary value problem for the radiation and scattering potentials. The use of Green's integral theorem yields hypersingular integrals (HIs) in terms of the jump in potential across the sides of each flap, which are solved using a numerical approach in terms of the Chebyshev polynomial of the second kind. The derivation of the mathematical model is quite general: one can solve for the unknown jump in potential across each flap for arbitrary configurations of the array. A wave farm consisting of various layouts of a finite array of OWSCs is then studied considering complete hydrodynamic interaction among all the devices.

The first theoretical model based on HIs was developed for an OWSC in a channel [10] and was then extended to study the hydrodynamics of an infinite array of WECs [11], a single device in the open ocean [12] and a finite array of in-line converters [9]. Recently, the same method was also used to analyse the hydrodynamics of a flap-type device near a straight coast [13]. Following the same approach, in this study we develop a mathematical model to investigate the hydrodynamic behaviour for the most generalised case consisting of a large number of OWSCs in any configuration with oblique wave incidence.

The generalised mathematical model is derived in the first part of the paper (§2 & §3). In §4, the effect of the separation distance is studied in detail using three flaps. This is followed by an analysis of both a wave farm comprising of thirteen flaps in various possible arrangements and a wave farm of 40 inline flaps. Finally the semi-analytical model is employed to study the hydrodynamics of two devices located back to back - a configuration which has intrigued many (see [14]).

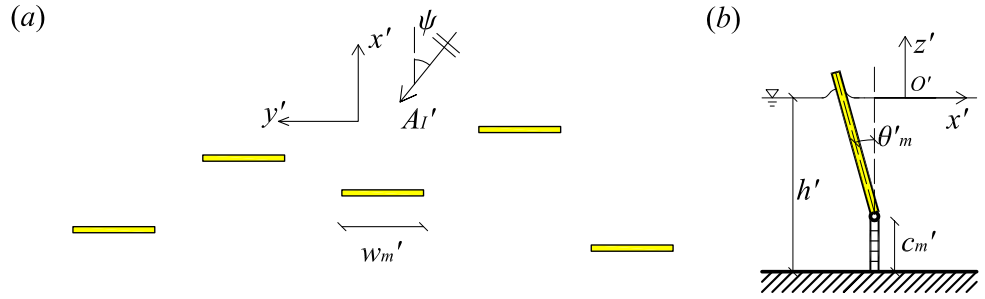

Figure 2. Geometry of the physical model of a portion of an OWSC array: (a) plan view; (b) section of the mth flap shown with the physical parameters.

2. Mathematical Model

(a) Governing Equations

A wave farm of M OWSCs is considered to be located in an ocean of constant water depth h'. Waves are incident from the right making an angle ψ with the $x'-$axis as shown in figure 2. The origin is located on the mean free surface with y' the pitching axis of the flaps and z' directed upwards. Primes in this mathematical model are used to denote the physical variables. With the assumption of irrotational flow and inviscid, incompressible fluid, the velocity potential Φ' satisfies the Laplace equation

$$\nabla'^2\Phi' = 0, \tag{2.1}$$

in the fluid domain, where $\nabla' f' = (f'_{,x'}, f'_{,y'}, f'_{,z'})$ is the nabla operator; subscripts with commas denote differentiation with respect to relevant variables. The linearised kinematic-dynamic boundary condition on the free surface gives

$$\Phi'_{,t't'} + g\Phi'_{,z'} = 0, \qquad z' = 0, \tag{2.2}$$

where g is the acceleration due to gravity while the no-flux boundary condition at the sea bed yields

$$\Phi'_{,z'} = 0, \qquad z' = -h'. \tag{2.3}$$

Each device is equipped with an oscillating flap hinged to a rigid foundation at a distance c' above the seabed (see again figure 2). The WECs are modelled using a thin-rigid plate approximation (see [15]) and the kinematic boundary condition on their surface is then expressed as

$$\Phi'_{,x'} = -\theta_{m,t'}(z' + h' - c')H(z' + h' - c'), \qquad x' = x'_m \pm \varepsilon', \varepsilon' \to 0,$$
$$y_m^{A'} < y' < y_m^{B'}, \quad m = 1, .., M, \tag{2.4}$$

where x'_m is the x' coordinate of the centre of the mth flap while $y_m^{A'}$ and $y_m^{B'}$ are the y' coordinates corresponding to the two edges of the device.

Like in previous work ([3,9–13]), a non-dimensional system of variables is chosen as

$$(x, y, z, r) = (x', y', z', r')/w', t = \sqrt{\frac{g}{w'}}t', \Phi = \frac{\Phi'}{\sqrt{gw'}A'_I}, \theta_m = (w'/A'_I)\theta'_m, \tag{2.5}$$

where w' is the length scale of the system (e.g. the width of the largest flap) and A'_I is the amplitude of the incident wave. Assuming the oscillation of the flaps to be simple harmonic in

nature, the time dependence of the variables can be separated out as

$$\theta_m = Re\{\Theta_m \exp^{-i\omega t}\}, \qquad \Phi = Re\{\phi(x,y,z)\exp^{-i\omega t}\}, \tag{2.6}$$

where $\omega = \omega'\sqrt{w'/g}$ and Θ_m are respectively, the angular frequency and amplitude of oscillation of the mth flap, while $\phi(x,y,z)$ is the complex spatial velocity potential. The spatial potential can in turn be resolved into

$$\begin{aligned}\phi &= \phi^S + \phi^R \\ &= \phi^I + \phi^D + \sum_{\beta=1}^{M} V_\beta \phi^{(\beta)}\end{aligned} \tag{2.7}$$

where

$$\phi^I = -\frac{iA_I}{\omega}\frac{\cosh k(z+h)}{\cosh kh}\exp^{-ikx\cos\psi + iky\sin\psi} \tag{2.8}$$

is the incident wave potential. In (2.7), ϕ^D is the diffracted wave potential, $\phi^{(\beta)}$ is the radiation potential induced by the motion of the β-th flap while the other flaps are held fixed and $V_\beta = i\omega\Theta_\beta$ is the complex angular velocity of the moving flap. Also note, in 2.8, k is the solution to the dispersion relation $\omega^2 = k\tanh kh$. On substitution of the factorisation (2.6) and (2.7) in the governing equations (2.1)–(2.4), we obtain a boundary value problem in terms of the spatial radiation and scattering potentials. These potentials satisfy the Laplace equation

$$\nabla^2\phi^{(\beta,D)} = 0, \tag{2.9}$$

where the notation $\phi^{(\beta,D)}$ denotes either potential, the linearised free-surface boundary condition

$$-\omega^2\phi^{(\beta,D)} + \phi^{(\beta,D)}_{,z} = 0, \qquad z = 0, \tag{2.10}$$

the no-flux boundary conditions at the sea bed

$$\phi^{(\beta,D)}_{,z} = 0, \qquad z = -h, \tag{2.11}$$

and the kinematic conditions on the lateral surfaces of the flaps

$$\begin{cases} \phi^{(\beta)}_{,x} = (z+h-c)H(z+h-c)\delta_{\beta m}, \quad x = x_m \pm \varepsilon, \varepsilon \to 0, \quad y^A_m \le y \le y^B_m, & (2.12) \\ \phi^D_{,x} = -\phi^I_{,x} & (2.13) \end{cases}$$

for $\beta = 1, 2, \cdots, M$, δ_{nm} being the Kronecker delta. Finally, both $\phi^{(\beta)}$ and ϕ^D are required to be outgoing disturbances of the wave field [16]. The vertical dependence can now be isolated out of the three dimensional governing system (2.9)–(2.13) by using the separation (see [9,12,16]):

$$\phi^{(\beta,D)}(x,y,z) = \sum_{n=0}^{\infty}\varphi_n^{(\beta,D)}(x,y)Z_n(z), \tag{2.14}$$

where

$$Z_n(z) = \frac{\sqrt{2}\cosh\kappa_n(z+h)}{(h+\omega^{-2}\sinh^2\kappa_n h)^{1/2}}, \quad n = 0, \cdots, \infty, \tag{2.15}$$

are the normalised vertical eigenmodes satisfying the orthogonality relation

$$\int_{-h}^{0} Z_n(z)Z_m(z)dz = \delta_{nm}. \tag{2.16}$$

In (2.15), $\kappa_0 = k$ and $\kappa_n = ik_n$ are the solutions of the dispersion relation

$$\omega^2 = k\tanh kh, \quad \omega^2 = -k_n\tanh k_n h, \quad n = 1, 2, \cdots, \tag{2.17}$$

respectively.

Using the decomposition (2.14) and the orthogonality relation (2.16) yields a two-dimensional governing system for $\varphi_n^{(\beta,D)}$, where the Laplace equation (2.9) becomes the Helmholtz equation

$$(\nabla^2 + \kappa_n^2) \left\{ \begin{array}{c} \varphi_n^\beta \\ \varphi_n^D \end{array} \right\} = 0, \tag{2.18}$$

and the kinematic conditions on the flap (2.12) become

$$\left\{ \begin{array}{c} \varphi_{n,x}^\beta \\ \varphi_{n,x}^D \end{array} \right\} = \left\{ \begin{array}{c} f_n \delta_{\beta m} \\ A_I d_n^m e^{iky\sin\psi} \end{array} \right\} \qquad x = x_m \pm \varepsilon, \varepsilon \to 0, \quad y_m^A < |y| < y_m^B, \tag{2.19}$$

where

$$f_{n\beta} = \frac{\sqrt{2}[\kappa_n(h-c)\sinh(\kappa_n h) + \cosh(\kappa_n c) - \cosh(\kappa_n h))]}{\kappa_n^2(h + \omega^{-2}\sinh^2(\kappa_n h))^{1/2}} \tag{2.20}$$

and

$$d_n^m = \frac{k\cos\psi(h+\omega^{-2}\sinh^2 kh)^{1/2}}{\sqrt{2}\omega\cosh kh}[\cos(kx_m\cos\psi) - i\sin(kx_m\cos\psi)]\delta_{0n} \tag{2.21}$$

are integration constants depending on the geometry of the system. Finally the $\varphi_n^{(\beta,D)}$ must be outgoing disturbances for $r \to \infty$. The boundary value problem (2.18) – (2.19) is solved with the application of Green's integral theorem, similar to the procedure followed in [10]. The formulation yields HIs which are solved using the Chebyshev polynomials of the second kind (see Appendix A for details). Finally the solution for the β-th mode radiation potential is obtained as

$$\begin{aligned} \phi^{(\beta)}(x,y,z) = -\frac{i}{8}\sum_{n=0}^{+\infty}\kappa_n x Z_n(z)\sum_{m=1}^{M} w_m \sum_{p=0}^{P} a_{pnm}^{(\beta)} \int_{-1}^{1}(1-u^2)^{1/2}U_p(u) \\ \times \frac{H_1^{(1)}\left(\kappa_n\sqrt{(x-x_m)^2 + (y - \frac{uw_m + 2y_m^C}{2})^2}\right)}{\sqrt{(x-x_m)^2 + (y-\frac{uw_m+2y_m^C}{2})^2}}du, \end{aligned} \tag{2.22}$$

where $w_m = y_m^B - y_m^A$ is the non-dimensional width of the mth flap, U_p is the Chebyshev polynomial of the second kind and order p, $p = 0, 1, \cdots, P \in \mathbb{N}$, $H_1^{(1)}$ is the Hankel function of the first kind and first order, y_m^C the y coordinate of the center of flap m while $a_{pnm}^{(\beta)}$ are the complex solutions obtained using a numerical collocation scheme (see Appendix A). The solution to the spatial diffraction potential is expressed as

$$\begin{aligned} \phi^D(x,y,z) = -\frac{i}{8}A_I k x Z_0(z)\sum_{m=1}^{M} w_m \sum_{p=0}^{P} b_{p0m} \int_{-1}^{1}(1-u^2)^{1/2}U_p(u) \\ \times \frac{H_1^{(1)}\left(k\sqrt{(x-x_m)^2 + (y - \frac{uw_m + 2y_m^C}{2})^2}\right)}{\sqrt{(x-x_m)^2 + (y-\frac{uw_m+2y_m^C}{2})^2}}du, \end{aligned} \tag{2.23}$$

where the b_{p0m} are the complex solutions of a system of equations, again solved numerically. Note that in ϕ^D (2.23) only the 0th order vertical mode is present, the flaps being walled structures in the scattering problem (i.e $\varphi_n^D = 0$ for $n > 0$). Using the above expressions (2.22) and (2.23), the equation of motion of the flap can be now solved.

(b) Hydrodynamic Parameters

The solution for the velocity potential is then used to solve the equation of motion of each individual flap in the frequency domain. Suppose for the α-th flap, $I_\alpha = I'_\alpha/(\rho w_\alpha'^5)$ is the second

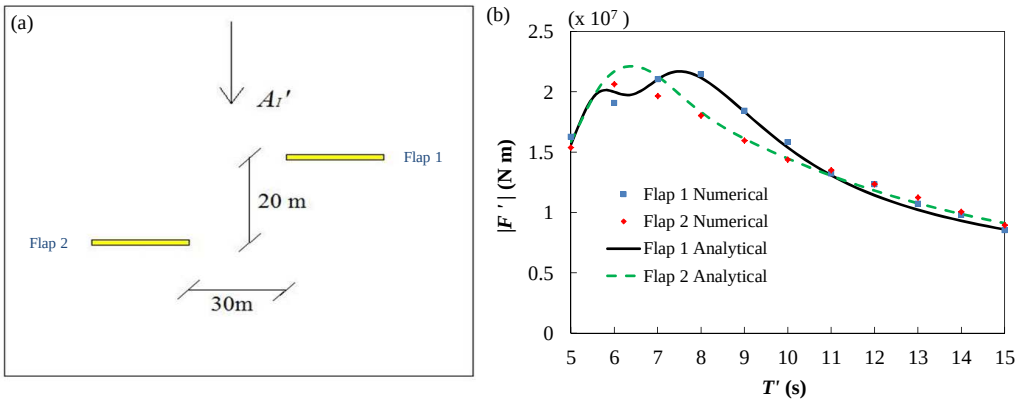

Figure 3. (a) Plan view of two OWSCs in a staggered configuration as analysed in [9]; (b) Comparison of excitation torque on two flaps versus incident wave period. The solid line and the dotted line represent the variation of F' of flap 1 and 2 respectively, obtained using the semi-analytical approach presented here, while the squares and the diamonds are from the numerical analysis presented in [9]. Results are shown for $A_I' = 1$m, $h' = 13$m, $w' = 26$m and $c' = 4$m.

moment of inertia and $C_\alpha = C_\alpha'/(\rho g w_\alpha'^4)$ is the coefficient of the flap restoring buoyancy torque. Then its non-dimensional equation of motion can be expressed as shown in [9]

$$[-\omega^2(I_\alpha + \mu_{\alpha\alpha}) + C_\alpha - i\omega(\nu_{\alpha\alpha} + \nu_\alpha^{pto})]\Theta_\alpha - \sum_{\beta=1}^{M}[\omega^2\mu_{\beta\alpha} + i\omega\nu_{\beta\alpha}]\Theta_\beta = F_\alpha\,. \tag{2.24}$$

In the latter,

$$\mu_{\beta\alpha} = \frac{\pi w_\alpha}{4} Re\left\{\sum_{n=0}^{\infty} f_{n\alpha} a_{0n\alpha}^{(\beta)}\right\} \tag{2.25}$$

is the added moment of inertia,

$$\nu_{\beta\alpha} = \frac{\pi\omega w_\alpha}{4} Im\left\{\sum_{n=0}^{\infty} f_{n\alpha} a_{0n\alpha}^{(\beta)}\right\} \tag{2.26}$$

is the radiation damping and

$$F_\alpha = -\frac{\pi\omega w_\alpha}{4} i A_I b_{00\alpha} f_{0\alpha} \tag{2.27}$$

is the excitation torque (see [9]). Also in (2.24), $\nu_\alpha^{pto} = \nu_\alpha^{pto'}/(\rho w_\alpha'^5\sqrt{g/w_\alpha'})$ is the power take-off (PTO) damping coefficient of the α-th flap and following [4], is set equal to the optimal PTO damping for the same OWSC isolated in the open ocean:

$$\nu_\alpha^{pto} = \sqrt{\frac{[C_\alpha - (I_\alpha + \mu_\alpha^{open})\omega^2)]^2}{\omega^2} + (\nu_\alpha^{open})^2}, \tag{2.28}$$

where μ_α^{open} and ν_α^{open} are respectively the added moment of inertia and radiation damping of the α-th OWSC isolated in the open ocean. According to the theory of damped oscillating systems (see [17]), the average extracted power by the wave farm over a wave period is

$$P = \frac{1}{2}\omega^2 \sum_{i=1}^{M} \nu_i^{pto}|\Theta_i|^2. \tag{2.29}$$

The performance of the system is measured with the interaction factor q, defined as the ratio of total power captured by an array of M flaps to the power captured by an isolated WEC of the

same type multiplied by M:

$$q = \frac{P}{MP_{single}}. \tag{2.30}$$

A value of $q > 1$ implies that there is a gain in the net power output from an array because of constructive interaction amongst the flaps. On the other hand, $q < 1$ indicates that mutual interactions have a cumulative destructive influence on the array efficiency. However, the interaction factor q (2.30) doesn't quantify the performance of individual array elements. In order to understand the performance dynamics of each WEC in an array, [4] defined a term q_m^{mod} given by

$$q_m^{mod} = \frac{P_m - P_{single}}{\max(P_{single})}, \qquad m = 1, 2, \cdots, M, \tag{2.31}$$

where P_m is the power captured by the mth flap while $\max(P_{single})$ is the maximum value of P_{single} in the considered range of incident wave periods. The parameter q_m^{mod} represents the array induced performance modification of each individual WEC, with $q_m^{mod} > 0$ implying a beneficial influence and $q_m^{mod} < 0$ a negative interaction effect. The two terms q and q_m^{mod} together can reasonably describe the global and single scale performance behaviour of an array configuration.

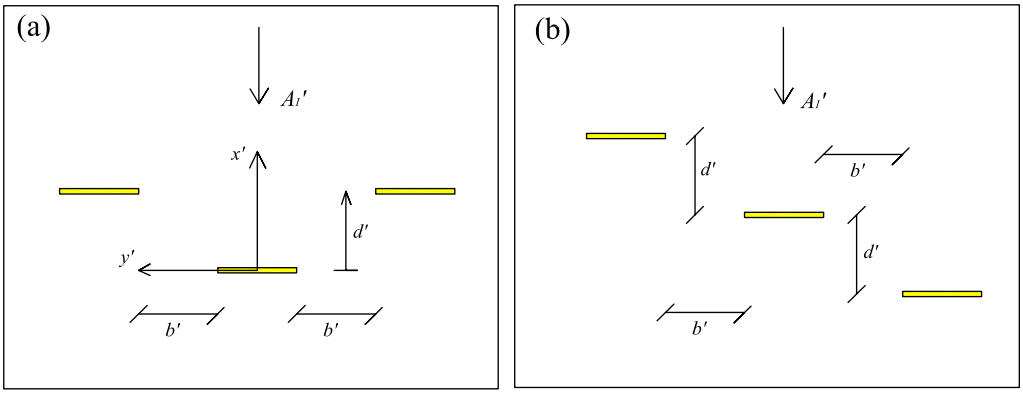

Figure 4. Two configurations of a three-flap array are shown here. In both cases the spacings are uniform and normal incidence is considered. In (a) the two lateral flaps are located along the same x' coordinate which makes the system symmetrical about the $x'-$axis while (b) represents a non-symmetrical configuration.

3. Algorithm implementation and computational cost

An algorithm based on the mathematical model described here has been implemented through a code written in Mathematica® 8. The algorithm and the code have been made as general as possible and can handle a large number of flaps in any staggered configuration. The code requires no modification if the number of flaps or their configuration/positions are changed. Only the coordinates of the flap centres need to be changed. The other required inputs to the code are the flap width, distance from the sea bottom to the hinge, water depth, incident wave amplitude, range and number of incident wave periods, angle of oblique wave incidence, moment of inertia and buoyancy torque of the flap and total number of vertical eigenmodes, order of Chebyshev polynomials and terms in the remainder of the Hankel function (see (A 8)). A relative error of $O(10^{-3})$ is obtained with the first three vertical eigenmodes and sixth-order Chebyshev polynomials. From a computational point of view, the semi-analytical approach described here is extremely efficient compared with a full numerical approach. The latter has been used in [9]

to model a three-flap inline and a two-flap staggered configurations. The computational expense associated with the full numerical approach was on an average 1 hour for a single wave period evaluation performed on a computer equipped with an i7 2.67 GHz CPU and 12GB RAM. Computations with the semi-analytical model presented here were performed with an i7 3.40 GHz CPU and 16GB RAM equipped computer. For the assessment of a system of thirteen flaps only six minutes are required in average for each wave period.

4. Results

The computations are performed for several configurations of OWSCs, each one closely resembling the Oyster800 WEC developed by Aquamarine Power Ltd. The parameters of the system are reported in Table 1.

Table 1. Dimension of the physical variables

A_I'	w'	h'	c'
0.3m	26m	13m	4m

In the following, we shall validate the computational model with available theoretical and numerical results. Then we will discuss the interactions arising in a simple three-flap cluster and further show the potential of the model in handling more complex and populated arrays.

(a) Validation

The solution obtained for an inline array ($x_m = 0$, $m = 1, 2, \cdots, M$) of flaps and normal incidence ($\psi = 0^\circ$) is exactly the same as shown in [9] and consequently the same results are obtained for the two-flap inline and three-flap inline cases as presented in [9]. For staggered configurations, results for only two flaps are available in literature and have been obtained with a numerical tool [9]. Figure 3 shows the variation of the excitation torque versus time period of the incident wave for the two-flap staggered case of [9]. A fairly consistent agreement is observed in the results obtained by the current model and the numerical approach of [9].

(b) Three-flap cluster

In order to understand the effects of the mutual interactions arising in a wave farm, we first consider a basic array cluster comprising of only three flaps and we focus our attention on the performance of the flap positioned centrally amongst them. This central flap in a way represents an OWSC located well within an array, where the hydrodynamic influences of only its two neighbouring devices are dominant. We consider both symmetrical and non-symmetrical configurations of the three flaps with essentially uniform spacing between them in normally incident waves.

Let us first consider the case of the symmetrical configuration shown in figure 4(a). Here the distance d', measured from the central flap, is positive in the positive $x'-$direction. Therefore $d' > 0$m represents the case when the central flap is located behind the two lateral flaps, while $d' < 0$m indicates otherwise. Figure 5 plots the q_2^{mod} of the central OWSC for various distances of separation. Each of the sub-plots shows the behaviour for a particular value of the lateral distance b' while varying d'. It can be observed that $d' > 0$m is associated with a strong destructive influence on the central flap's performance across the entire operating range of periods. On the other hand, for $d' < 0$m, positive interaction effects dominate and significantly enhance the

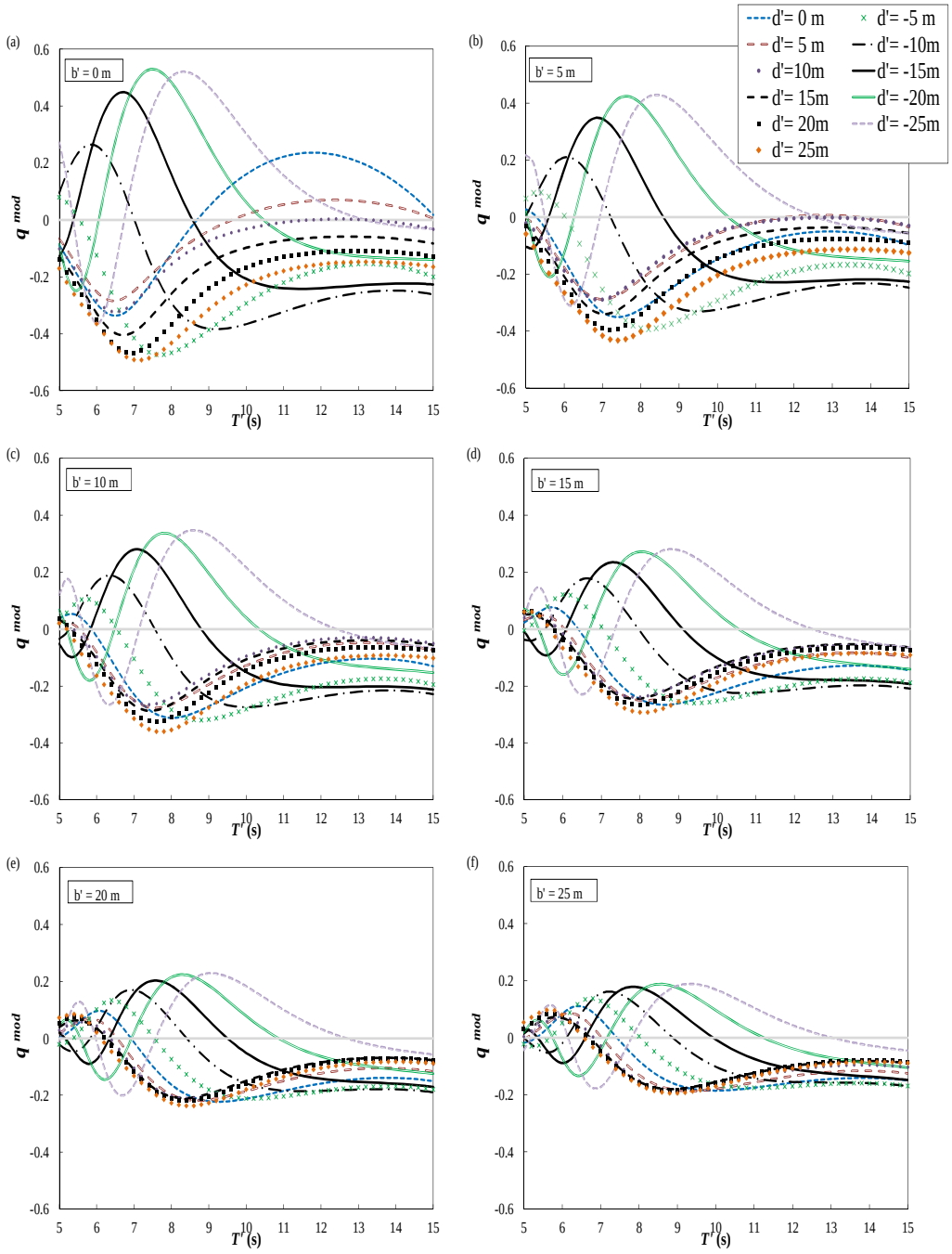

Figure 5. Variation of q_2^{mod} versus incident wave period for the central flap for the symmetrical three-flap cluster configuration shown in figure 4(a). Each of the sub-plots shows the q_2^{mod} variation for a particular value of b' while the distance d' is varied.

performance of the central flap, suggesting that an OWSC will have better power absorption characteristics when located at the front of the cluster. The most important thing to note is that for the situations considered here, the qualitative behaviour of the q^{mod} variation is determined by d', while b' primarily dictates the extent of the peaks (see again figure 5). In general, as the distance

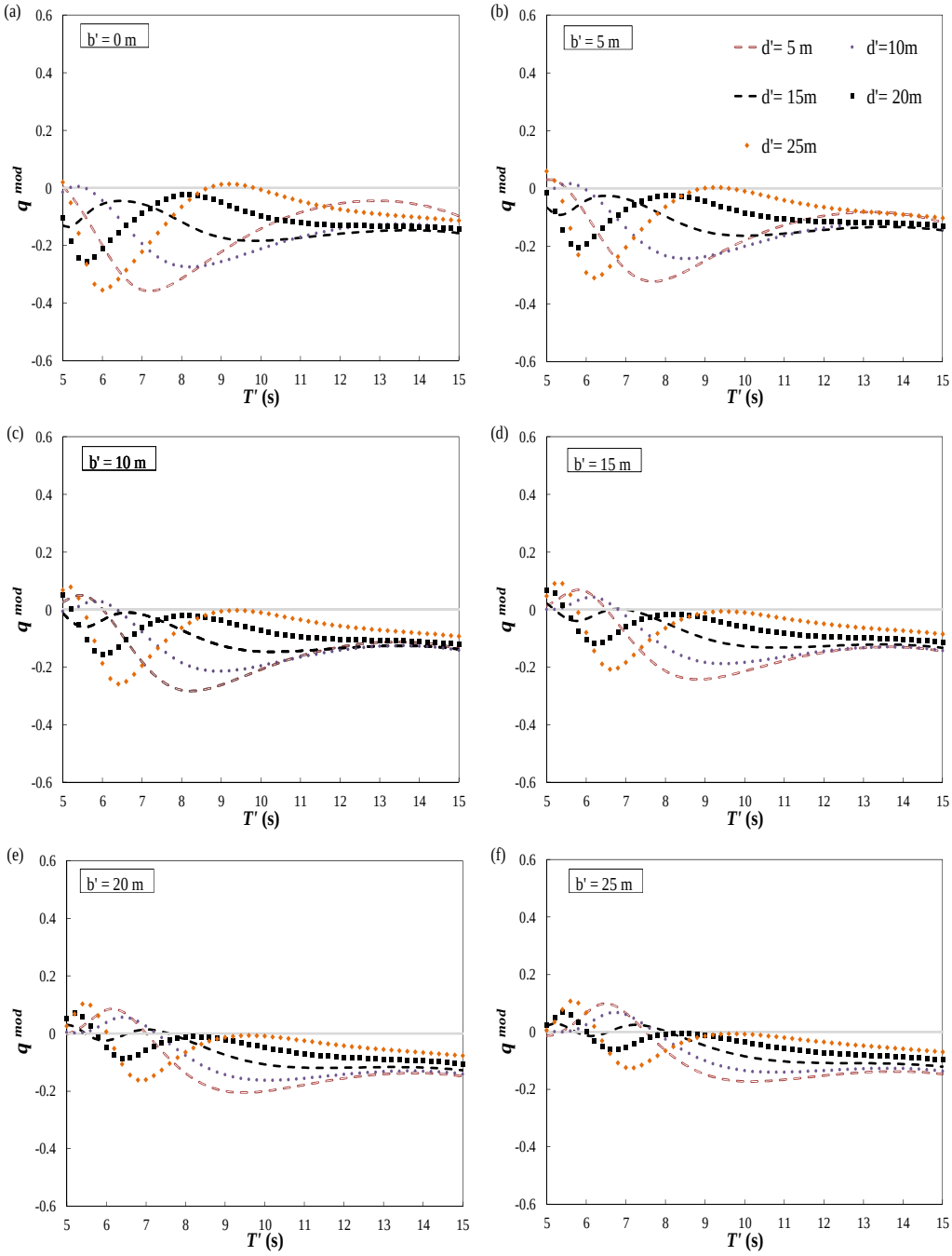

Figure 6. Variation of q_2^{mod} versus the incident wave period of the central flap for the non-symmetrical 3-flap cluster configuration shown in figure 4 (b). Each of the sub-plots shows the q_2^{mod} variation for a particular value of b' while the distance d' is varied.

b' is increased there is a shift in the q^{mod} variations towards higher periods, accompanied by a reduction in the magnitude of the peaks, which means a decrease in the interaction amongst the flaps. It can be inferred that as b' is further increased, there would be a larger number of local maxima and minima of reduced magnitudes and so on average, there would be no distinctive

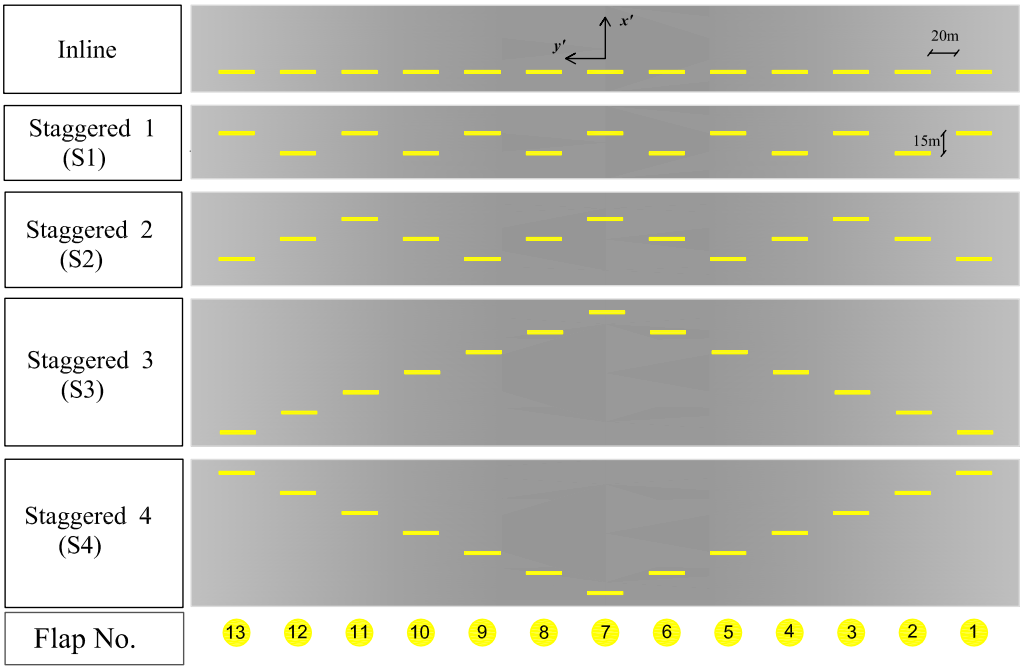

Figure 7. Five possible layouts of a 13 OWSC wave farm are shown here. The magnitude of the spacings between neighbouring flaps in all the cases is fixed at 20m in the $y-$direction and 15m in the $x-$direction.

positive or negative interaction effect on the device performance for any value of d'.

Now we consider the case where the layout of the flaps with respect to the centreline of the middle OWSC is non-symmetrical, as shown in figure 4(b). The noticeable difference with the previous arrangement is that the pitching axes of the extreme flaps are now separated from that of the central flap in opposite directions. The q_2^{mod} variation of the central flap for the various cases is plotted in figure 6. Almost ubiquitously for the range of distances considered, such a configuration has a negative influence on the WECs performance. This is likely due to the opposite interaction effects on the central OWSC by the two lateral flaps.

(c) Wave farm of 13 OWSCs

A wave farm consisting of 13 flaps in various configurations is shown in figure 7. Typically even larger arrays could be studied using the same computational infrastructure mentioned previously within a reasonable time. The spacing between the flaps is chosen similar to the one planned for the proposed wave farm at the Isle of Lewis in Scotland [1]. For the purpose of identifying each individual converter, the flaps are numbered in an increasing order from right to left of the array with the OWSC located on the extreme right considered as flap 1. The distance between the edges of the neighbouring flaps is 20m in the $x'-$direction for all the configurations shown in figure 7, while the pitching axes of the neighbouring flaps in the staggered configurations are separated by a distance of 15m. The wave farms considered in the analysis are symmetrical about the central flap (flap 7), so for normal wave incidence the hydrodynamic behaviour is symmetric with respect to the $x'-$axis passing through the center of the central flap.

Inline: The inline case corresponds to the configuration in which the pitching axes of all the flaps are oriented along the same x' coordinate. As first described by [9], a near resonant behaviour is observed in this case which is similar to the resonance of an infinite array of inline OWSCs [11] or a single OWSC in an open channel [10] (see figure 8a). At the near resonant period, the performance of every individual OWSC is higher than in the isolated case and q^{mod} has a peak for

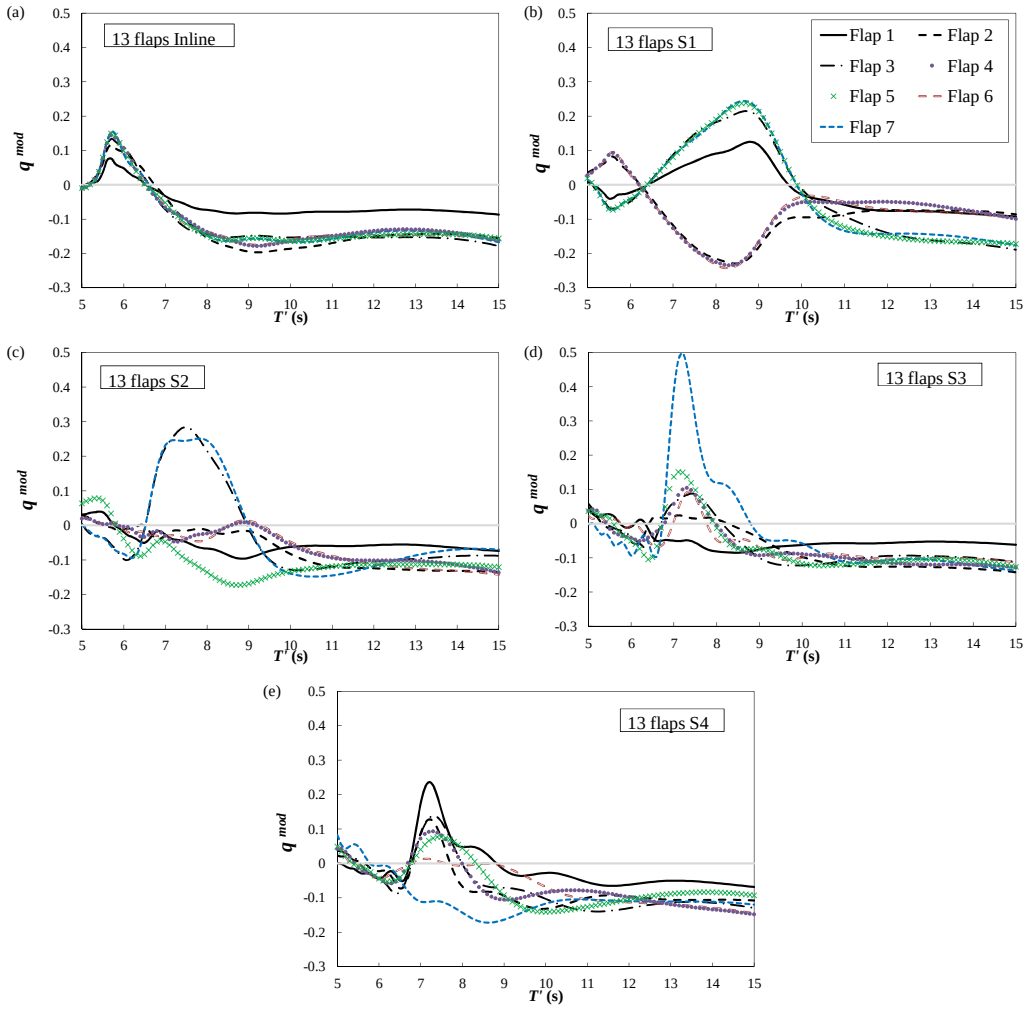

Figure 8. Variation of q^{mod} of the individual OWSCs for the five layouts shown in figure 7. Since normal wave incidence is considered here, the configuration is symmetrical about the central flap and the results are plotted for only seven flaps. Flap 1 is the OWSC located in the extreme right of the array shown in figure 7 while Flap 7 is the central flap.

all the flaps. However such a behaviour is also accompanied by destructive influences at higher periods. Amongst all the flaps, the outermost OWSC has a slightly distinguishable behaviour from the others. This is due to the fact that while all the other OWSCs have neighbouring flaps on both sides which generate the maximum influence, the outermost flap only experiences the hydrodynamic influence of the converters located on one side. Let us now consider a case of oblique wave incidence on inline OWSCs. As expected, the behaviour of the wave farm is no longer symmetrical about its innermost flap. Figures 9(a) and (b) show the q^{mod} of all the 13 flaps when $\psi = 30^{\circ}$. A similar near resonant behaviour is observed in this case as well. However, the strongest near-resonant behaviour occurs for flap 1 and the magnitude of the peaks reduces as one moves towards the other end of the array, with flap 13 showing a distinctively different behaviour.

S1: In such a configuration, the OWSCs are placed in a zigzag manner with the array comprising of two rows of devices. The flaps located in the same row have similar hydrodynamic behaviour, as seen in figure 8(b) . Flaps 3, 5 & 7, which are positioned in the front, have almost the same

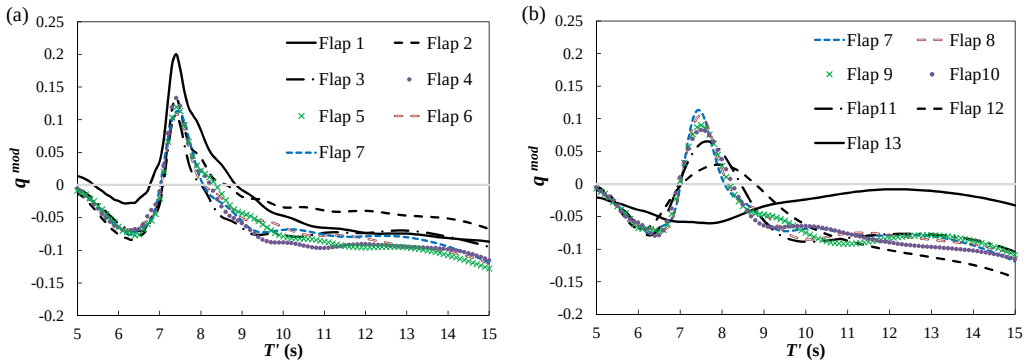

Figure 9. Variation of q^{mod} of 13 flaps in an inline configuration for oblique wave incidence $\psi = 30°$: (a) Flap 1 to Flap 7; (b) Flap 7 to Flap 13.

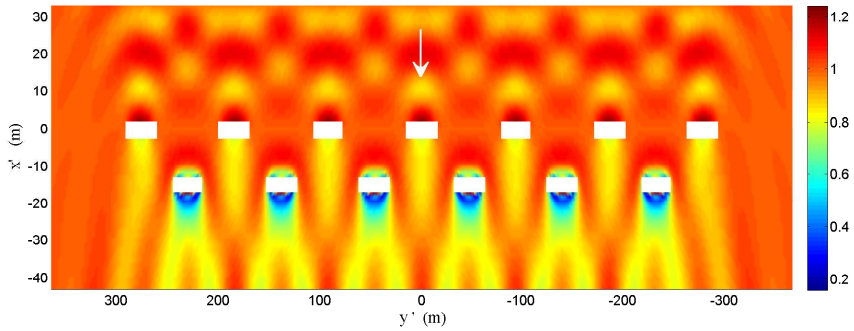

Figure 10. Response amplitude operator (RAO) of the free surface elevation in a wave farm of 13 flaps in the staggered S1 configuration shown in figure 7 for an incident wave period $T' = 5$sec.

q^{mod} variation and similar are the behaviours of flaps 2, 4 & 6. However, the performance characteristics of the flaps in the two rows are in striking contrast, with the maxima in q^{mod} of the OWSCs in the front row corresponding to the minima of the OWSCs in the back row and vice versa. This happens since a flap in the front row experiences the maximum constructive interaction, as already anticipated in the cluster analysis of §4(b). Figure 10 plots the response amplitude operator (RAO) of the free surface elevation ($|\zeta'/A'_I|$) for an incident wave period of 5 seconds in the region surrounding the wave farm. There is hardly any noticeable change in the wave field in front of the array, but in the immediate wake behind the WECs there is a strong reduction in the wave elevation, meaning a less energetic wave field available for extraction by the back row.

S2: Here the devices are again placed in a zigzag distribution but now there are three rows in this configuration. Flaps 3 and 7 are located in front of the array and experience a beneficial influence due to constructive interactions leading to relatively high values of q^{mod} (see figure 8c). One can again note the similarity in the behaviour of the OWSCs in the second row (flaps 2, 4 and 6). Finally, flap 5, the only non-external flap to be located on the last row, has a predominantly negative q^{mod} factor. The behaviour is indeed similar to that obtained from the corresponding configurations of the three-flap cluster of §4(b).

S3: The layout of this array resembles an inverted 'V' shape, pointing away from the coast. Figure

8(d) shows the q^{mod} variation of the flaps in such a configuration. The most striking behaviour is of the foremost WEC (flap 7). Indeed, one could have expected it to have a positive q^{mod} factor based on the behaviour observed in the cluster model of §4(b). However, the magnification of the q^{mod} factor in this case is further enhanced by what we believe to be a strong focussing effect. In the S3 configuration (see again figure 7) all the flaps behind the central one reflect back some amount of incident wave energy. As a consequence, more energy is available for extraction by the foremost device (flap 7), resulting in the peak of the relevant q^{mod} in figure 8(d). A further insight into such dynamics is offered by figure 12, which shows the excitation torque on the flaps in the S3 configuration. The variation of the excitation torque is similar to that of the q^{mod} factor of figure 8(d) and one can notice a sharp increase in $|F'|$ for flap 7 at the same peak period ($T' \sim 7.2s$). Such a behaviour again corroborates the well known fact that the dynamics of the OWSCs like Oyster is primarily torque-driven (see [3,10,12]).

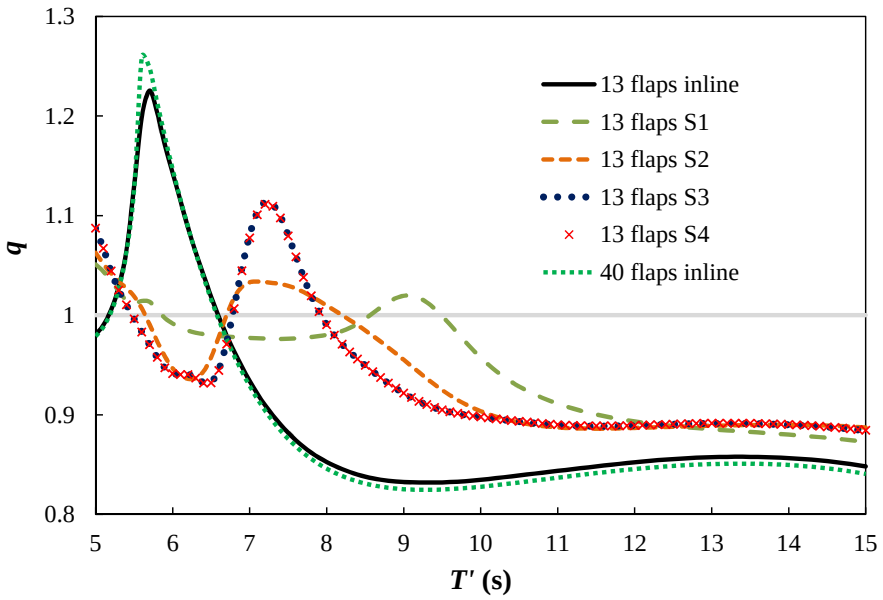

Figure 11. Variation of the performance parameter q for the five different layouts of 13 flaps as shown in figure 7 and an inline layout of a wave farm comprising of 40 flaps.

S4: Here again the outermost flaps, which are located in the front, record the highest peak in the q^{mod} factor (see figure 8e). However, although the configuration mirrors to the previous one, there is no such equivalent constructive focussing effect on the central flap (flap 7).

An overview of the general behaviours of all the systems is provided in figure 11. Here the variation of the global performance parameter q (2.30) is plotted against the period of the incident wave. Overall, the strongest constructive interaction is achieved in the inline system, while the staggered systems S1 and S2 show the least constructive interference between the flaps, mainly due to the poor performance of the back row because of the sheltering effect of the front row (e.g. see figure 10). This confirms the earlier findings of [9] for a smaller system. Finally, the configurations S3 and S4, for which the net power output is the same, show a smaller peak than the inline configuration, but an overall better performance according to the q indicator. It is worth to mention that our analysis is based purely on the hydrodynamic performance of the system. Other aspects (environmental impact, site bathymetry, etc.) could of course orient the designer towards a less effective configuration from the hydrodynamic viewpoint. Nevertheless, such a

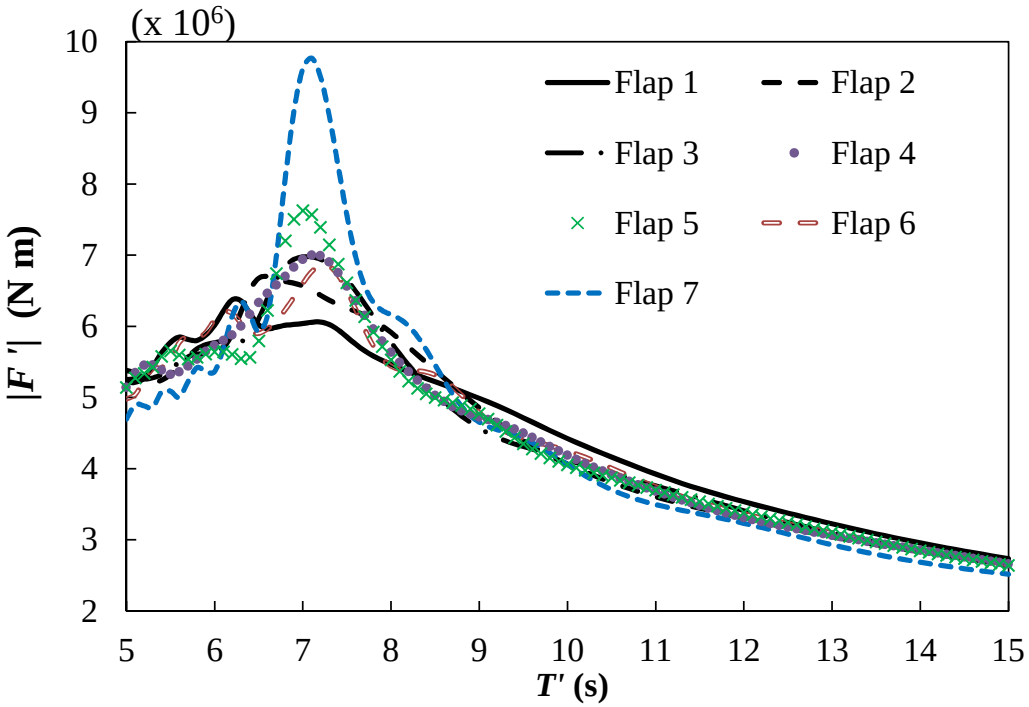

Figure 12. Behaviour of the excitation torque $|F'|$ on individual flaps versus incident wave period for a 13-flap array in the staggered S3 configuration.

hydrodynamic analysis is a first step towards the effective design of such a costly system.

(d) 40 flaps inline

The proposed 40MW wave farm off the north-west coast of Lewis, Scotland is expected to have a deployment of around 40 to 50 Oyster devices on an approximate 3.2 kilometre stretch of coast. In order to check the reproducibility of the results obtained from the small wave farm cases in such large configurations, a simulation of 40 OWSCs in a simple inline configuration is performed. The general geometry is considered to be the same as in the 13 flap configuration. In figure 11 the variation of the q factor for the 40 flap configuration is plotted. The behaviour is indeed similar to that of the 13 flap inline case and the near-resonant behaviour is again confirmed with a slightly larger spike tending towards that of an infinite number of OWSCs (see again [9] and [11]). It can be reasonably inferred that the general behaviour in other configurations would be similar to that in the smaller wave farm case with sharper spikes and troughs.

(e) Two flaps back to back

Two flaps with their centres along the same y' coordinate are studied here (see figure 13). It is expected that such a configuration would result in strong hydrodynamic interaction between the two devices. [14] were the first to analyse the behaviour of two top hinged independently oscillating rolling plates in deep waters as a WEC. The novel concept motivated a few other studies [18], where one of the major drawbacks of such system was identified to be its strong directional sensitivity to wave incidence and the concept was thereafter shelved. Surprisingly, the idea was not pursued in shallow waters where the waves are predominantly directional. In this study we are going to explore if it is wise to place two OWSCs back to back.

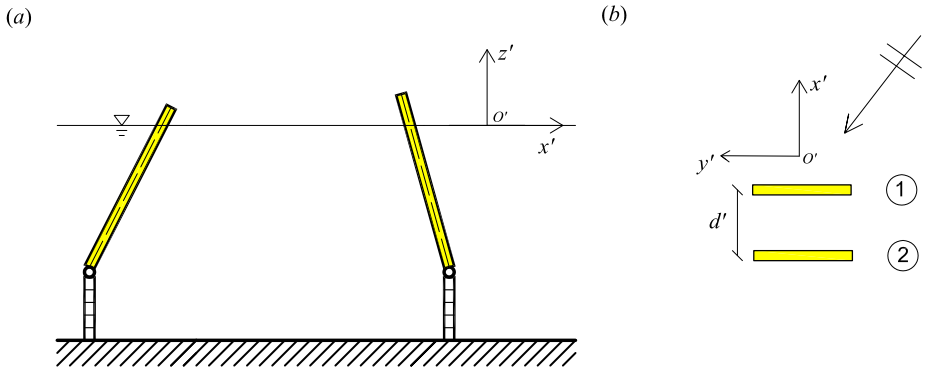

Figure 13. Geometry of the physical model of two back to back OWSCs: (a) side view; (b) top view. The distance of separation between the flaps is denoted by d' in this case.

Figure 14 plots the behaviour of the excitation torque ($|F'|$), radiation damping (ν'), added inertia (μ') and the performance indicator q^{mod} versus the non-dimensional parameter kd for $d' = 50$m. The qualitative variation of the hydrodynamic parameters of the front flap has resemblance to that observed in the case of an OWSC in front of a straight coast [13]. In the latter, periodic occurrences of extremes are observed in the variation of the excitation torque, with the minima occurring at integral values of kd/π. Also, sharp spikes are observed in the variation of the radiation parameters at values a little less than $kd = (m + 1/2)\pi$, $m = 1, 2, \cdots$. In the case of the two flaps analysed here, the hydrodynamic behaviour of the front OWSC is similar to that of a flap in front of a straight coast, with however, reduced peaks and a shift where the extremes occur.

As far as the performance of the devices is concerned, the average value of q^{mod} of Flap 1 is higher than that of Flap 2 (see figure 14(b)). The constructive interference effects on Flap 1 are very strong at $kd \approx 5$ where q^{mod} almost reaches a value of 0.5. Flap 2 (back OWSC) always captures less power than a single isolated OWSC, which means that the interaction effects are always destructive on its performance. The primary reason for such a behaviour is that the back flap lies in the wake field created by the front flap where the wave energy is reduced. Figure 14 shows the variation of q for various values of the distance d'. For $d' = 25$m, the destructive interaction effects are quite significant and $q \approx 0.5$ at an incident wave period of about 6 seconds. This means that the total power captured by the two devices combined at that frequency is equivalent to the energy extracted by an isolated single device. As the distance d' is increased, the occurrence of the humps in the variation of q increases but the magnitude of such deviations reduces as well. The most important thing to note is that the constructive interference effects are much weaker compared to destructive influences and on an average the two OWSCs in such a configuration capture less power than two isolated WECs.

(f) Two Wave Farms

In reality, an ideal wave energy site may encourage the deployment of two consecutive wave farms for energy harvesting. It is important to understand the dynamics of the system in such cases especially with one of the wave farm lying in the energy shadow of the other. A simplified case of two inline wave farm configurations, each comprising of 13 flaps is considered in normal wave incidence (see figure 16). The analysis is performed in constant water depth to understand the dominant interaction effects between the systems, although in reality, variations in depth are expected to modify the behaviour slightly. The term q_{farm} is utilised to understand the effect of

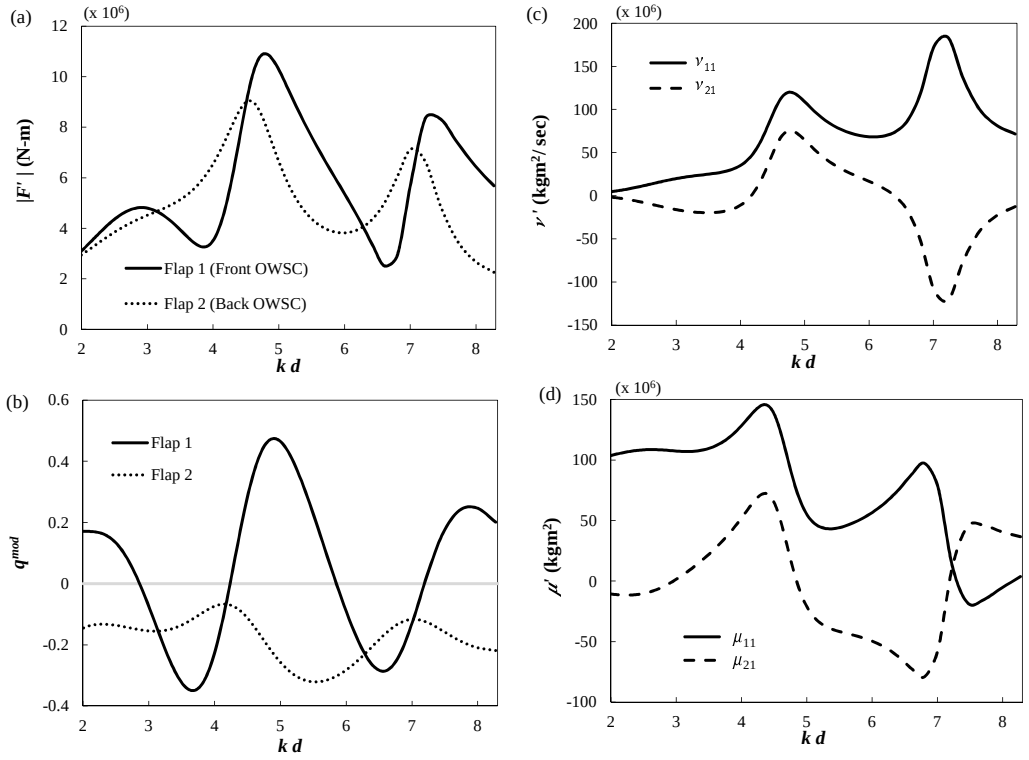

Figure 14. Behaviour for the case of two back to back OWSCs shown in figure 13 versus the non dimensional parameter kd for $d' = 50$m. (a) Magnitude of the excitation torque ($|F'|$); (b) Radiation damping (ν'); (c) q^{mod}; (d) Added inertia (μ').

the interaction on each of the wave farms and is defined as

$$q_{farm} = \frac{P_{farm}}{P_{farmisolated}}, \tag{4.1}$$

where P_{farm} is the total power captured by a particular wave farm while $P_{farmisolated}$ is that by the same farm in an isolated environment. $q_{farm} > 1$ would mean that the presence of the other farm has a net beneficial influence on power absorption characteristics of the particular wave farm considered, while $q_{farm} < 1$ indicates otherwise. Figure 17 plots the variation of q_{farm} versus the incident wave period of the two wave farms for various distances of separation. The oscillatory behaviour of the q_{farm} factor is similar to that of the q factor observed in the two back-to-back OWSCs case (see figure 15), with a higher number of such oscillations occurring for larger distances of separation. For the range of distances considered, the q_{farm} factor of wave farm 1 is always less than 1 which indicates that such configurations will tend to have a detrimental influence on the farm located nearer to the shore. However, a steady upward shift in the q_{farm} factor of wave farm 1 is observed as the distance is increased which can be explained due to the energy recovery in the wake of wave farm 2. The rate of energy recovery is in fact quite slow and even for a distance of 2000 m, the q_{farm} factor is still below 1. On the other hand, wave farm 2 has both detrimental and favourable interference effects. However, the magnitude of the oscillations in its q_{farm} factor is much higher than that in wave farm 1. It is interesting that the bandwidths of the oscillations are almost the same for the distances considered.

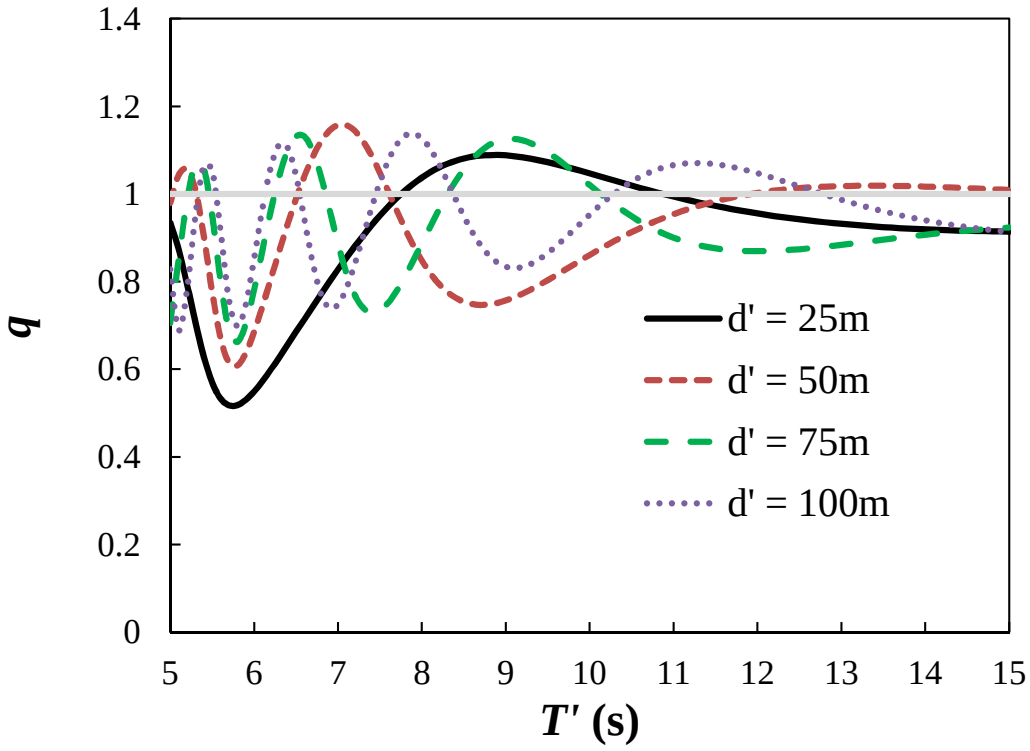

Figure 15. Variation of q versus incident wave period for the case of two back to back OWSCs with various values of separation distance d'.

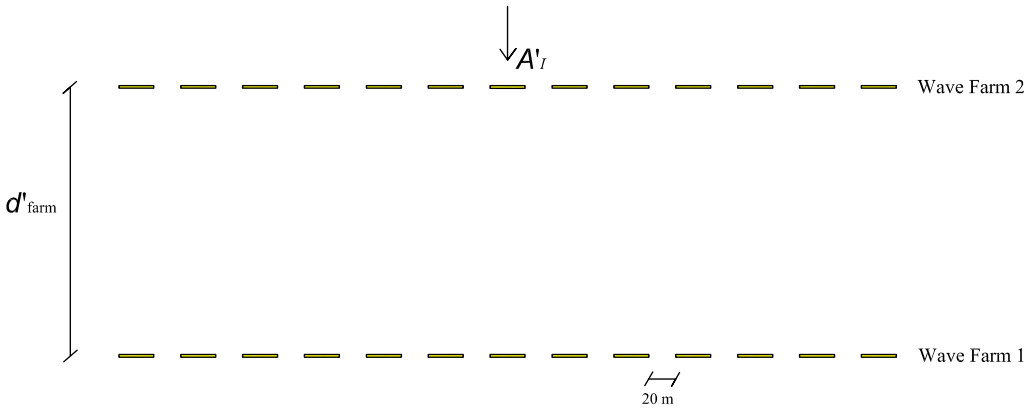

Figure 16. Layout of the two inline wave farm configurations separated by a distance d'_{farm}.

5. Conclusion

A mathematical model based on the linear potential flow theory has been used to analyse the hydrodynamic interaction between multiple flap-type WECs in a wave farm. The semi-analytical model can efficiently solve a reasonably sized OWSC wave farm which otherwise is difficult to evaluate with a complete numerical approach. It is shown that the dynamics of each individual OWSC in the wave farms considered in the analysis strongly depends on its location in the farm, the wave frequency and the angle of oblique wave incidence. As the distance between the flaps

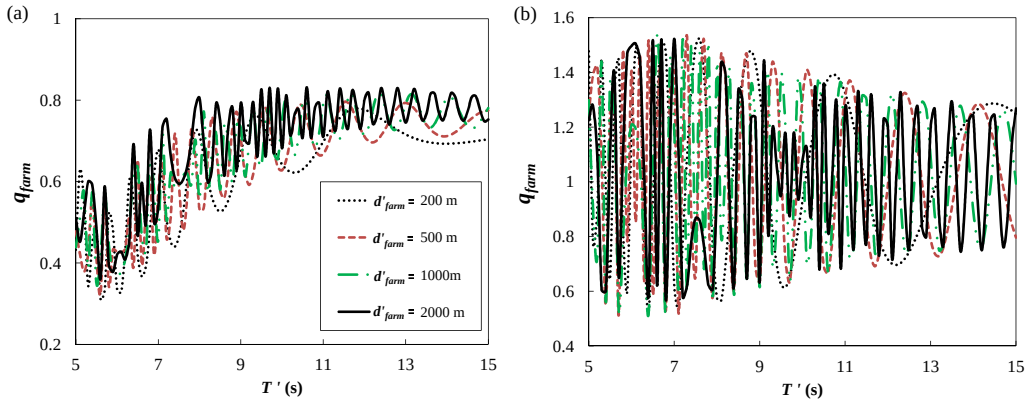

Figure 17. Variation of q_{farm} versus incident wave period for (a) wave farm 1 and (b) wave farm 2.

increases, the mutual hydrodynamic interaction between them reduces and the behaviour of the converters tends towards that of an isolated device. However, from an economic perspective, one would want to maximise the number of devices at a particular wave farm location to extract more power. This is important for nearshore devices like OWSCs as the space would be strictly limited unlike for offshore converters.

Wave absorption by an array of 13 OWSCs is studied for some of its possible layouts. For an inline configuration with normal incidence, a near resonant phenomenon is observed which becomes stronger as the number of flaps is increased. However, for oblique wave incidence there is a shift in the frequency of occurrence of this phenomenon with a slight increase in the resonant bandwidth associated with it. In a particular configuration of the large array (S3), a large enhancement in the performance of the front-most flap is observed. Such a behaviour is attributed to a sharp increase in the excitation torque due to the focussing of waves by the other devices in the array. In general, the converters which are located in front of the array experience a noticeable positive interaction effect leading to a gain in their power capture. Such a favourable behaviour in the performance of the foremost devices of the array is also reported in the recent study of [8]. In the case of two back to back OWSCs located close to each other, the effect on the performance of the back flap is found to be detrimental across its entire operating range, while the front OWSC experiences regions of both positive and negative influences. And when two such flaps are considered as one system, the destructive interference effects are found to be more important than the constructive influences. Therefore such a system of two OWSCs is not recommended in reality. Also it is shown that a system of two consecutive wave farms has in general a negative interaction effect on the net performance of the wave farm located downstream.

In a practical wave farm design however, the layout of an array configuration could be constrained by bathymetry variations which would affect the optimisation process. Although no particular layout could be suggested which would lead to a gain in net wave farm energy output across the entire operating range of the device, since the constructive interference effects are usually accompanied by destructive influences as well, the study can help understand what sort of variability in the performance of individual OWSCs one can expect.

Acknowledgment

The authors would like to thank Science Foundation Ireland for the financial support to the research project (No.:10/IN.1/I2996) "High-end computational modelling for wave energy systems". Dr. G. Bellotti and Mr. A. Abdolali are kindly acknowledged for the provision of the numerical data.

A. Semi-analytical Solution

The procedure to obtain the solution to the 2D spatial diffraction and radiation potential is described in this section. Consider the 2D Green's function

$$G_n(x,y;\xi,\eta) = \frac{1}{4i}H_0^{(1)}(\kappa_n\sqrt{(x-\xi)^2+(y-\eta)^2}), \tag{A 1}$$

which satisfies the system of equations

$$(\nabla^2+\kappa_n^2)G_n = 0, \qquad G_n = \frac{1}{2\pi}\ln r \quad as \quad r\to 0, \tag{A 2}$$

where $r=\sqrt{(x-\xi)^2+(y-\eta)^2}$. Applying Green's integral theorem to φ_n and G_n for the whole fluid domain yields

$$\varphi_n(x,y) = -\frac{i}{4}\sum_{m=1}^{M}\int_{y_m^A}^{y_m^B}\Delta\varphi_{nm}G_{n,\xi}^{(0)}\Big|_{\xi=x_m}d\eta, \tag{A 3}$$

where $\Delta\varphi_{nm}=\varphi_n(x_m-\varepsilon,y)-\varphi_n(x_m+\varepsilon,y)$ denotes the modal potential difference across the two sides of flap m. Applying the 2D spatial potential on the kinematic boundary conditions on the flaps, gives (see [9])

$$\begin{aligned}
&⨍_{y_\alpha^A}^{y_\alpha^B}\left\{\begin{array}{c}\Delta\varphi_{n\alpha}^{(\beta)}\\ \Delta\varphi_{n\alpha}^{D}\end{array}\right\}\frac{H_1^{(1)}(\kappa_n|y-\eta|)}{|y-\eta|}\kappa_n d\eta+\sum_{\substack{\gamma=1\\ \gamma\neq\alpha}}^{M}\int_{y_\gamma^A}^{y_\gamma^B}\left\{\begin{array}{c}\Delta\varphi_{n\gamma}^{(\beta)}\\ \Delta\varphi_{n\gamma}^{D}\end{array}\right\}\\
&\frac{-\kappa_n}{(x_\alpha-x_\gamma)^2+(y-\eta)^2}\Bigg[\kappa_n(x_\alpha-x_\gamma)^2\Bigg\{H_2^{(1)}(\kappa_n\sqrt{(x_\alpha-x_\gamma)^2+(y-\eta)^2})\\
&-\frac{H_1^{(1)}(\kappa_n\sqrt{(x_\alpha-x_\gamma)^2+(y-\eta)^2})}{\kappa_n\sqrt{(x_\alpha-x_\gamma)^2+(y-\eta)^2}}\Bigg\}-\frac{(y-\eta)^2}{\sqrt{(x_\alpha-x_\gamma)^2+(y-\eta)^2}}\\
&\times H_1^{(1)}(\kappa_n\sqrt{(x_\alpha-x_\gamma)^2+(y-\eta)^2})\Bigg]d\eta \quad = \quad 4i\left\{\begin{array}{c}f_{n\beta}\delta_{\alpha\beta}\\ A_I d_n^{(\alpha)}e^{iky\sin\psi}\end{array}\right\},
\end{aligned} \tag{A 4}$$

where ⨍ is a Hadamard finite-part integral. Let $y_m^C=(y_m^A+y_m^B)/2$ denote the y coordinate of the center of flap m, $m\epsilon[1,M]$. Making the following change of variables

$$u=\frac{2(\eta-y_m^C)}{w_m}, \qquad v_m=\frac{2(y-y_m^C)}{w_m}, \qquad \left\{\begin{array}{c}P_{n\alpha}^{(\beta)}(u)\\ Q_{n\alpha}(u)\end{array}\right\}=\left\{\begin{array}{c}\Delta\varphi_{n\alpha}^{(\beta)}\\ \Delta\varphi_{n\alpha}^{D}\end{array}\right\}, \tag{A 5}$$

yields

$$\begin{aligned}
&⨍_{-1}^{1}\left\{\begin{array}{c}P_{n\alpha}^{(\beta)}(u)\\ Q_{n\alpha}(u)\end{array}\right\}\frac{H_1^{(1)}(\frac{\kappa_n w_\alpha}{2}|v_\alpha-u|)}{|v_\alpha-u|}\kappa_n du+\sum_{\substack{\gamma=1\\ \gamma\neq\alpha}}^{M}\int_{-1}^{1}\left\{\begin{array}{c}P_{n\alpha}^{(\beta)}(u)\\ Q_{n\alpha}(u)\end{array}\right\}\\
&\frac{-\kappa_n 2w_\gamma}{4(x_\alpha-x_\gamma)^2+w_\gamma(v_\gamma-u)^2}\Bigg[\kappa_n(x_\alpha-x_\gamma)^2\Bigg\{H_2^{(1)}(\frac{\kappa_n}{2}\sqrt{(x_\alpha-x_\gamma)^2+w_\gamma(v_\gamma-u)^2})\\
&-\frac{2H_1^{(1)}(\frac{\kappa_n}{2}\sqrt{4(x_\alpha-x_\gamma)^2+w_\gamma^2(v_\gamma-u)^2})}{\kappa_n\sqrt{4(x_\alpha-x_\gamma)^2+w_\gamma^2(v_\gamma-u)^2}}\Bigg\}-\frac{w_\gamma^2(v_\gamma-u)^2}{2\sqrt{4(x_\alpha-x_\gamma)^2+w_\gamma^2(v_\gamma-u)^2}}\\
&\times H_1^{(1)}(\frac{\kappa_n}{2}\sqrt{4(x_\alpha-x_\gamma)^2+w_\gamma^2(v_\gamma-u)^2})\Bigg]du \quad = \quad 4i\left\{\begin{array}{c}f_{n\beta}\delta_{\alpha\beta}\\ A_I d_n^{(\alpha)}e^{ik(v_\alpha w_\alpha/2+y_\alpha^C)\sin\psi}\end{array}\right\}
\end{aligned} \tag{A 6}$$

Now

$$H_1^{(1)}\left(\frac{\kappa_n}{2}w_\alpha|v_\alpha-u|\right)=\frac{4}{i\pi}\frac{1}{\kappa_n w_\alpha|v_\alpha-u|}+R_n\left(\frac{\kappa_n}{2}w_\alpha|v_\alpha-u|\right), \tag{A 7}$$

where

$$R_n(z) = J_1(z)\left[1 + \frac{2i}{\pi}\left(\ln\frac{z}{2} + \chi\right)\right] - \frac{i}{\pi}\left[\frac{z}{2} + \sum_{j=2}^{+\infty}\frac{(-1)^{j+1}(z/2)^{2j-1}}{j!(j-1)!}\left(\frac{1}{j} + \sum_{q=1}^{j-1}\frac{2}{q}\right)\right] \tag{A 8}$$

is the remainder, J_1 is the Bessel function of first kind and first order, and $\chi = 0.577215\cdots$ is the Euler constant [10]. Expanding the unknown jumps in potential across the two sides of the flap as

$$\left\{\begin{array}{c} P_{nm}^{(\beta)}(u) \\ Q_{nm}(u) \end{array}\right\} = (1-u^2)^{1/2}\sum_{p=0}^{+\infty}\left\{\begin{array}{c} a_{pnm}^{(\beta)} \\ A_I b_{pnm} \end{array}\right\} U_p(u), \tag{A 9}$$

where a_{pn} and b_{pn} are unknown complex coefficients to be determined and $U_p(u)$ is the Chebyshev polynomial of second kind, finally gives

$$\sum_{p=0}^{\infty}\left\{\left\{\begin{array}{c} a_{pn\alpha}^{(\beta)} \\ b_{pn\alpha} \end{array}\right\} C_{np}(v_\alpha) + \sum_{\substack{\gamma=1 \\ \gamma\neq\alpha}}^{M}\left\{\begin{array}{c} a_{pn\gamma}^{(\beta)} \\ b_{pn\gamma} \end{array}\right\} D_{np}(v_\alpha)\right\} = -\pi w_\alpha\left\{\begin{array}{c} f_n\delta_{\alpha\beta} \\ d_n^{(\alpha)} e^{ik(v_\alpha w_\alpha/2 + y_\alpha^C)\sin\psi} \end{array}\right\} \tag{A 10}$$

where

$$C_{pn\alpha} = -\pi(p+1)U_p(v_\alpha) + \frac{i\pi\kappa_n w_\alpha}{4}\int_{-1}^{1}(1-u^2)^{1/2}U_p(u)\frac{R_n\left(\frac{1}{2}\kappa_n|v_\alpha - u|\right)}{|v_\alpha - u|}du, \tag{A 11}$$

$$\begin{aligned} D_{pn\alpha\gamma} = -\frac{i\pi\kappa_n w_\alpha}{4}\int_{-1}^{1}\frac{(1-u^2)^{1/2}U_p(u)2w_\gamma}{4(x_\alpha - x_\gamma)^2 + (v_\alpha w_\alpha + 2y_\alpha^C - 2y_\gamma^C - w_\gamma u)^2} \\ \left[(x_\alpha - x_\gamma)^2\left\{\kappa_n H_2^{(1)}\left(\frac{\kappa_n}{2}\sqrt{4(x_\alpha - x_\gamma)^2 + (v_\alpha w_\alpha + 2y_\alpha^C - 2y_\gamma^C - w_\gamma u)^2}\right)\right. \right. \\ \left. - \frac{2H_1^{(1)}\left(\frac{\kappa_n}{2}\sqrt{4(x_\alpha - x_\gamma)^2 + (v_\alpha w_\alpha + 2y_\alpha^C - 2y_\gamma^C - w_\gamma u)^2}\right)}{\sqrt{4(x_\alpha - x_\gamma)^2 + (v_\alpha w_\alpha + 2y_\alpha^C - 2y_\gamma^C - w_\gamma u)^2}}\right\} \\ - \frac{(v_\alpha w_\alpha + 2y_\alpha^C - 2y_\gamma^C - w_\gamma u)^2}{2\sqrt{4(x_\alpha - x_\gamma)^2 + (v_\alpha w_\alpha + 2y_\alpha^C - 2y_\gamma^C - w_\gamma u)^2}} \\ \left. H_1^{(1)}\left(\frac{\kappa_n}{2}\sqrt{4(x_\alpha - x_\gamma)^2 + (v_\alpha w_\alpha + 2y_\alpha^C - 2y_\gamma^C - w_\gamma u)^2}\right)\right]du \end{aligned} \tag{A 12}$$

$$v_\alpha = \frac{\cos(2q+1)\pi}{2P+2}, \qquad q = 0, 1, 2, \cdots, P\,. \tag{A 13}$$

In the case of an inline array configuration, $x_\alpha = x_\beta$ and the term D_{pn} indeed reduces to

$$D_{pn\alpha\gamma} = \frac{i\pi\kappa_n w_\alpha w_\gamma}{4}\int_{-1}^{1}(1-u^2)^{1/2}U_p(u) \times \frac{H_1^{(1)}\left(\frac{\kappa_n}{2}|v_\alpha w_\alpha + 2y_\alpha^C - 2y_\gamma^C - uw_\gamma|\right)}{|v_\alpha w_\alpha + 2y_\alpha^C - 2y_\gamma^C - uw_\gamma|}du, \tag{A 14}$$

and correspond to the term (A.12) of [9]. Further generalising it for normal incidence reduces the system of equations (A 10) exactly to (A.10) of [9].

References

1. Aquamarine Power Limited 2012 *Lewis Wave Power 40 MW Oyster Wave Array Non Technical Summary*. See http://www.aquamarinepower.com.
2. Budal, K. 1977 Theory for absorption of wave power by a system of interacting bodies. *J. Ship Res.* **21**,4.
3. Renzi, E. , Doherty, K. , Henry, A. & Dias, F. 2013 How does Oyster work? The simple interpretation of Oyster mathematics. *Eur. J. Mech. B/Fluids* (submitted).
4. Babarit, A. 2010. Impact of long separating distances on the energy production of two interacting wave energy converters. *Ocean Eng.* **37**,718-729.
5. Cruz, J., Sykes, R., Siddorn, P. & Eatock Taylor, R. 2009 Wave farm design: preliminary studies on the influences of wave climate, array layout and farm control. *Proceedings of the European Wave and Tidal Energy Conference, Uppsala, Sweeden.*
6. Child, B.F.M. & Venugopal, V. 2010 Optimal configurations of wave energy device arrays. *Ocean Eng.* **37**,1402–1417.
7. Wolgamot, H.A., Taylor, P.H., & Eatock Taylor, R. 2012 Optimal configurations of wave energy device arrays. *Ocean Eng.* **47**,65-73.
8. Borgarino, B., Babarit, A. & Ferrant, P. 2012 Impact of wave interactions effects on energy absorption in large arrays of wave energy converters. *Ocean Eng.* **49**,79-88.
9. Renzi, E., Abdolali, A., Bellotti, G. & Dias, F. 2014 Wave-power absorption from a finite array of Oscillating Wave Surge Converters. *Renewable Energy* **63**,55-68.
10. Renzi, E. & Dias, F. 2012 Resonant behaviour of an oscillating wave energy converter in a channel. *J. Fluid Mech* **701**,482-510.
11. Renzi, E. & Dias, F. 2013 Relations for a periodic array of flap-type wave energy converters. *Appl. Ocean Res.* **39**,31-39.
12. Renzi, E. & Dias, F. 2013 Hydrodynamics of the Oscillating Wave Surge Converter in the open ocean. *Eur. J. Mech. B/Fluids* **41**,1-10.
13. Sarkar, D., Renzi, E. & Dias, F. 2013 Effect of a straight coast on the hydrodynamics and performance of an Oscillating Wave Surge Converter. *Submitted* .
14. Srokosz, M.A. & Evans, D.V. 1979 A theory for wave-power absorption by two independently oscillating bodies. *J. Fluid Mech* **90**,337–362.
15. Linton, C. M. & McIver, P. 2001 *Handbook of mathematical techniques for wave/structure interactions.* Chapman & Hall/CRC.
16. Mei, C.C., Stiassnie, M. & Yue, D.K.P. 2005 *Theory and Applications of Ocean Surface Waves.* World Scientific.
17. Falnes, J. 2002 *Ocean Waves and Oscillating Systems.* Cambridge University Press.
18. Scher, R.M., Troesch, A.W., & Zhou, G. 1983 The experimental and theoretical evaluation of a twin-flap wave-energy absorbing device. *Ocean Eng.* **10**,325-345.